Materials Horizons

ROYAL SOCIETY OF CHEMISTRY

COMMUNICATION

View Article Online
View Journal | View Issue

Cite this: *Mater. Horiz.*, 2022, 9, 1273

Received 26th November 2021,
Accepted 3rd February 2022

DOI: 10.1039/d1mh01918j

rsc.li/materials-horizons

Polymer dielectric films exhibiting superior high-temperature capacitive performance by utilizing an inorganic insulation interlayer†

Tiandong Zhang,[a] Lianyin Yang,[a] Changhai Zhang,[a] Yu Feng,[a] Jian Wang,[b] Zhonghui Shen,*[b] Qingguo Chen,[a] Qingquan Lei[a] and Qingguo Chi*[a]

With the rapid development of next-generation electrical power equipment and microelectronics, there is an urgent demand for dielectric capacitor films which can work efficiently under extreme conditions. However, sharply increased electrical conduction and drastically degrading electric breakdown strength are inevitable at elevated temperatures. Herein, a facile but effective method is proposed to improve high temperature capacitive performance. We report that utilizing an inorganic insulation interlayer can significantly increase the discharge energy density with a high efficiency above 90% at 150 °C, *i.e.*, a discharged energy density of 4.13 J cm^{-3} and an efficiency of >90% measured at 150 °C, which is superior to the state-of-the-art dielectric polymers. Combining the experimental results and computational simulations reveals that the remarkable improvement in energy storage performance at high temperature is attributed to the blocking effects that reduce the leakage current and maintain the breakdown strength. The proposed facile method provides great inspiration for developing polymer dielectric films with high capacitive performance under extreme environments.

New concepts

The serious degradation of energy at elevated temperature is one of the most important challenges for the application of dielectric capacitors. In this work, we propose a new method to improve energy storage performance at high-temperature. We utilize an insulation interlayer to reduce electrical conduction and enhance electric breakdown strength of polymer dielectric films. This facile but effective method significantly improves the high temperature capacitive performance. The discharge energy density with high efficiency above 90% at 150 °C, *i.e.*, a discharged energy density of 4.13 J cm^{-3} and an efficiency of >90% measured at 150 °C, is superior to the state-of-the-art dielectric polymers. This is the first demonstration of the application of an inorganic interlayer for a new type of dielectric capacitor. The proposed facile method and meaningful findings offer great inspiration for developing polymer dielectric films with high capacitive performance under extreme environments.

1. Introduction

Polymer-based dielectric films are commonly used as a key component in energy storage capacitors due to being lightweight, flexible, low cost, with scalable production and high tolerance to voltage.[1–6] However, the serious degradation of energy storage performance under harsh environments, such as a high electric field or high temperature, is causing a bottleneck.[7–9] For example, biaxially oriented polypropylene (BOPP) film is the most popular commercial dielectric capacitor film, but its energy loss sharply increases when it works at a temperature higher than 80 °C, failing to meet the requirement of next-generation capacitors above 150 °C.[10] It is widely accepted that the electrical conduction loss mainly contributes to the decrease of discharge energy density (U_e) and efficiency (η), resulting from the increased leakage current (J) and the degraded electric breakdown strength (E_b), so how to suppress the electrical conduction loss of the dielectric films under high electric field and at elevated temperature has become a key issue.

In recent years, researchers proposed some effective strategies to improve the capacitive performance of the polymer films at elevated temperature, including: (1) developing new polymer dielectric films. Zhang *et al.* synthesized a new kind of dipolar glass polymer – sulfonylated poly(2,6-dimethyl-1,4-phenylene oxide) (abbreviated as SO_2-PPO) – which possesses a glass transition temperature (T_g) of 200 °C and ultralow dielectric loss ($\tan\delta \sim 0.003$), U_e reached 2.2 J cm^{-3} at 150 °C when η remained above 90%;[11] sulfonylated organo-soluble polymers of intrinsic microporosity (SO_2-PIM) were also successfully fabricated and had a high performing energy storage

[a] School of Electrical and Electronic Engineering, Harbin University of Science and Technology, Harbin, China. E-mail: qgchi@hrbust.edu.cn
[b] International School of Materials Science and Engineering, Wuhan University of Technology, Wuhan, China. E-mail: zhshen@whut.edu.cn

† Electronic supplementary information (ESI) available. See DOI: 10.1039/d1mh01918j

performance at 150 °C, $U_e \sim 2.75$ J cm^{-3} and $\eta \sim 93\%$.[12] (2) Modifying the molecular structure of the polymer. It was reported that the crosslinked structures acted as molecular trapping centers and inhibited the charge transport in the polymer at elevated temperatures. The cross-linked poly(chlorotrifluoroethylene-*co*-vinylidene fluoride) (abbreviated as XL-VK) demonstrated good capacitive performance at high temperature, a U_e of 2.67 J cm^{-3} with an η of $> 90\%$ at 150 °C.[13] Using the saturated fused bicyclic structure in the backbone instead of aromatic structures, the polyoxafluoronorbornene (POFNB) film endowed a large bandgap of $\sim$5 eV and exhibited electrical conductivity two orders of magnitude lower than commercial polymer films.[14] (3) Adding functional fillers into the polymer. Either inorganic fillers with a wide bandgap[15–19] or semi-conductive organic fillers with high electron affinity,[18] both of which are beneficial to incorporating trap centers, limiting charge transport and reducing electrical conduction loss. A U_e of 3.31 J cm^{-3} and $\eta > 90\%$ at 150 °C were obtained in the polymer-based nanocomposites filled with Al_2O_3 nanoplates.[15] Similarly, poly(arylene etherurea) (PEEU) filled with a ultra-low content of 0.21 vol. % Al_2O_3 nanoparticles could generate a high U_e of 5 J cm^{-3} with $\eta > 90\%$ at 150 °C.[16] In addition, the molecular semiconductors, such as PCBM, could impede electric charge injection and transport dielectric polymers *via* strong electrostatic attraction, giving polyetherimide (PEI) a U_e of 3 J cm^{-3} with $\eta > 90\%$ at 200 °C.[20] (4) Constructing the multilayer structure. The multilayer films were designed by combining the different functionality of the individual layers, and the capacitive performances at elevated temperature can be improved. In particular, the energy barrier at the electrodes/dielectric film could be enhanced by coating a barrier layer with a wide bandgap, such as SiO_2, BN or Al_2O_3, leading to significantly suppressed electrical conduction and improved energy storage performance.[21–23] The maximum U_e value at $\eta > 90\%$ for SiO_2/PEI/SiO_2 multilayer films was 2.12 J cm^{-3} at 150 °C, far exceeding the film without an SiO_2 layer.[10] Furthermore, the sandwich-structured films consisting of the high polarization layer and high breakdown strength layer, simultaneously had high dielectric constant and low dielectric loss, and a U_e of 1.1 J cm^{-3} with an η of 93% have been achieved in sandwich-structured polymer nanocomposites at 150 °C.[24]

The above-mentioned effective methods are anticipated to reduce the electrical conduction loss, suppress the leakage of current density and improve tolerance to electric fields at high temperature, thus a desirable capacitive performance would be obtained. However, the following issues should also be further considered: the synthesis of a new polymer may be time-consuming and costly – it is a long way from discovery to application; the crosslinking byproducts and any negative impact on high temperature energy storage performance of the polymers needs to be steadfastly avoided; the uniform dispersion of functional nanofillers in the polymer matrix must be easily possible to enable industrial production; the complicated manufacturing for multilayer films should be simplified and the cost should be lowered. So, it is still urgent to find other effective ways to achieve scalable production, lower cost and to reduce electrical conduction loss in dielectric polymer films at high electric field and high temperature.

It has been proven by Huang *et al.* that sandwiching an ultrathin layer of a two-dimensional inorganic insulator between two polymer layers is an effective strategy to substantially improve the breakdown strength and energy storage performance of dielectrics.[25] In this study, a facile but effective method was proposed to improve energy storage performances at elevated temperatures. Here, PEI and an MgO inorganic functional layer with wide bandgap were chosen as the top/bottom polymer layer and the interlayer, respectively. Different from either the polymer nanocomposites with inorganic fillers or coated in an inorganic layer on the electrode/dielectric interface, the present work enables an inorganic layer to act as an interlayer between top/bottom PEI layers. Through regulating the thickness of the inorganic functional layer, the leakage current density is significantly suppressed and the electric breakdown strength is enhanced at elevated temperatures. In particular, the PEI/MgO/PEI (denoted as PMP) film delivers an ultrahigh U_e of 4.13 J cm^{-3} with an η above 90% at 150 °C, which is 335% that of the pristine PEI film and is also superior to the current reported polymer nanocomposites and other polymer-based multilayer films.

2. Experimental

2.1. Materials

The heat-resistant polymer dielectrics polyetherimide (PEI, $T_g \approx 217$ °C) was provided by PolyK Technologies. Magnesium oxide nanoparticles (MgO) with average particle size of 50 nm were purchased from AladdinA. Hexagonal boron nitride powder (h-BN) with average particle size of 1 μm was purchased from Sigma Aldrich Co., Ltd. Isopropanol was purchased from Tianjin Fuyu Chemial Co., Ltd. *N*-methyl pyrrolidone (NMP) was bought from Tianjin Bailunsi Biotechnology Co., Ltd. *N*,*N*-dimethylformamide (DMF) was bought from Sinopharm Chemical Reagent Co., Ltd.

2.2. Exfoliation of h-BN powder into BNNS

BNNS was fabricated *via* a modified liquid-phase exfoliation method. First, h-BN powder was added into DMF. Then this mixture was placed in a sonication bath for 48 h. The resulting solution was centrifuged at 8000 rpm for 20 min, and the precipitate was taken and freeze dried for 24 hours.

2.3. Preparation of sandwich-structured composite films

The sandwich-structured composite films were prepared through a layer-by-layer solution-casting process as shown in Fig. 1a. First, PEI particles were dissolved in NMP, and the magnetic stirrer temperature was set to 50 °C, and stirring was continued for 12 hours to obtain a uniform and stable suspension. Before casting onto a clean glass substrate, all the mixtures were put into a vacuum oven to remove the bubbles. Then, this mixture was cast onto a glass plate using a doctor

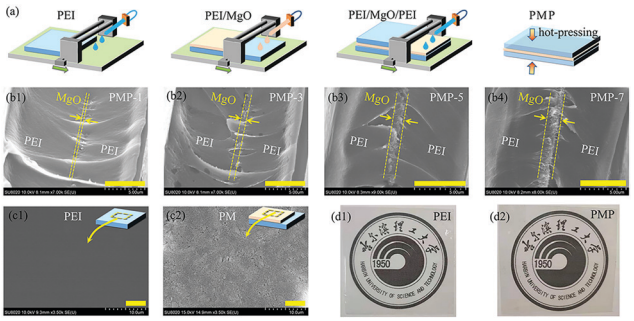

Fig. 1 (a) Schematic of the fabrication process of PMP films. (b) SEM images showing the cross-section structure of the PMP films. (c) Surface structure of PEI and PMP-5 films. (d) Optical images of PEI and PMP-5 films (all scale bars are 5 μm).

blade, and served as the first layer. The solution-cast films were kept in a drying oven at 70 °C for 6 h and then heated to 120 °C, 150 °C and 200 °C for 2 h, respectively. Afterwards, the films were dried in the vacuum oven at 200 °C for 2 h. Meanwhile, four different amounts of MgO (or BNNSs) were added into isopropanol and sonicated for 12 h to obtain a homogeneous solution (1, 3, 5, and 7 mg mL^{-1}). After the first PEI layer was fully dried, the MgO (or BNNSs) solution was cast as the second layer by the same process. Finally, after the isopropanol was completely removed, the third layer (PEI) was cast to the second layer, and dried in the same way as the first layer. According to the concentration of MgO (or BNNSs) solution, four kinds of sandwich structure film were recorded as PMP-1, PMP-3, PMP-5 and PMP-7 (or PBP-1, PBP-3, PBP-5 and PBP-7). The typical thickness of the prepared dielectric films used for electrical characterization was within the range of 12–15 μm.

2.4. Preparation of nanocomposites

The nanocomposites were fabricated through a solution casting process. MgO (or BNNSs) nanofillers with varied concentration (1 wt%, 3 wt%, 5 wt%, 7 wt%) were uniformly dispersed in NMP by magnetic stirring and ultrasonication for 4 h. And then the PEI particles were added in proportion and the magnetic stirrer temperature was set to 50 °C, and stirring was continued for 12 hours to obtain a uniform and stable suspension. All the mixtures were cast on a clean glass substrate after removing bubbles in the vacuum furnace. The solution-cast films were kept in a drying oven at 70 °C for 6 h and then heated to 120 °C, 150 °C and 200 °C for 2 h, respectively. Afterwards, the films were dried in the vacuum oven at 200 °C for 2 h. According to the concentration of MgO (or BNNSs), four kinds of nanocomposite films were recorded as PEI/MgO-1, PEI/MgO-3, PEI/MgO-5 and PEI/MgO-7 (or PEI/BN-1, PEI/BN-3, PEI/BN-5 and PEI/BN-7). The typical thickness of the prepared dielectric films used for electrical characterization was within the range 12–15 μm.

2.5. Characterization

The morphology of the fracture surfaces of the composite films was determined by field-emission scanning electron microscopy (SEM, SU 8020). The crystal structure of the composite films was analyzed by X-ray diffraction (XRD, Panalytical Empyrean). The molecular structure and chemical bonds of the polymer films were observed by Fourier transform infrared spectroscopy (FTIR, JASCO 6100). UPS was investigated using an X-ray photoelectron spectrometer (Thermo Fisher, ESCALAB 250Xi, USA). MgO powders were pasted onto the bottom of copper foil, PEI film was directly adhered to the conductive adhesive and then adhered to the sample table. The vacuum of the analysis chamber was about 2×10^{-8} mbar, the excitation source was HeI ultraviolet light, the excitation source energy was 21.22 eV, the working voltage was 12.5 kV, the filament current was 16 mA, and the signal was carried out through 5–10 cycles. An X-ray photoelectron spectrometer (KRATOS, Ultra DLD, UK) was used for XPS measurement. The MgO powder was pasted onto the conductive adhesive. The vacuum of the analysis chamber was 9.8×10^{-10} torr, and the excitation source was Al kα ray ($h\nu$ = 1486.6 eV). The full-spectrum acquisition voltage was 15 kV, the filament current was 5 mA, and the test energy pass energy was 160 eV; the fine spectrum voltage was 15 kV, the filament current was 10 mA, and the test energy pass energy was 40 eV. It is necessary to evaporate aluminum electrodes on both sides of the films before the electrical performance measurements, the circular electrode's diameter is 3 mm. The dielectric performance of the composite films from frequency 10^1 to 10^6 Hz was studied by a broadband dielectric spectrometer (Novocontrol GmbH, Germany). The electric displacement–electric field (D–E) loops were measured using a modified Sawyer-Tower circuit (Poly K, United States). The current density was characterized by a precision LC ferroelectric test system (Radiant Technologies, USA). In addition, the breakdown strength of thin films was tested by a DC breakdown test system (Poly K, United States), the ramping rate of breakdown strength test was 400 V s^{-1} and the cumulative breakdown probability was calculated by Weibull distribution. The cyclic fast charge–discharge tests were performed using a modified Sawyer-Tower circuit. The fast discharge tests were performed through a capacitor charge–discharge test system (Poly K, United States) with the load resistor of 10 kΩ.

3. Results and discussion

3.1. Fabrication and morphology characterization of PMP films

The fabrication process of the PEI film with MgO interlayer is illustrated in Fig. 1a. The MgO inorganic layer was fabricated using a solution casting method on the bottom surface of the PEI film, and then the inorganic interlayer was coated on the top of the PEI film: the PMP film was successfully prepared after undergoing the first three coating steps and the last hot-pressing step. Through changing the concentration of MgO solution with 1, 3, 5, and 7 g L^{-1}, the PMP-1, PMP-3, PMP-5 and PMP-7 films, respectively, were yielded. The morphology of the resultant films was characterized by SEM showing the cross-section structure of the PMP films, as given in Fig. 1b. The thickness of the MgO layer depends on the solution

concentration and increases gradually from 200 nm to 1400 nm for PMP-1, PMP-3, PMP-5 and PMP-7 films. Importantly, it can be seen that the MgO inorganic layer binds tightly with the top/bottom PEI layer, and no obvious defects between the PEI and MgO interfaces can be observed. MgO fillers unevenly dispersed in the PEI/MgO nanocomposites can be seen in the SEM results in Fig. S1–S3, ESI.† Fig. 1c shows the surface morphology where the MgO interlayer on the surface of the PEI film is a compact layer. Besides, no secondary phases in the PMP films can be detected from the XRD results in Fig. S4 (ESI†) and FTIR results in Fig. S5, ESI.† The optical images of the pristine PEI and PMP-5 films are shown in Fig. 1(d), indicating that the PMP film possesses excellent transparency after introducing an MgO interlayer comparable to the pristine PEI film.

3.2. Dielectric properties of PMP films

To investigate the effect of the MgO interlayer on the dielectric properties of the PMP films, the dielectric constant (ε_r) and dissipation factor ($\tan\delta$) as a function of frequency and temperature are given in Fig. 2a and b, respectively. It can be seen that the dielectric constant has good stability from 10 Hz to 10^6 Hz, with a minor variation in ε_r with increasing frequency, but is lower than the 4.3% variation for pristine PEI. We also see that ε_r of PMP films increases gradually with increasing thickness of the MgO interlayer, owing to the much higher dielectric constant of MgO ($\varepsilon_r \sim 9.8$)[26] than that of a PEI film ($\varepsilon_r \sim 3.15$ at10 Hz). This phenomenon can also be verified from the dielectric property of PEI/MgO nanocomposites, where the increased ε_r of the PEI filled with MgO nanoparticles is obtained, as given in Fig. S6, ESI.† As shown in Fig. 2b, at 1 kHz, ε_r of PMP films exhibits better stability with increasing temperature from 25 °C to 150 °C, for example, 2.64% for PMP-5 films. The dissipation factor increases gradually with increasing temperature as a whole, which may be attributable to the thermal-excited electrical conduction. However, the PMP-5 film still delivers a much lower dissipation factor, indicating that the appropriate thickness of MgO interlayer can reduce the dielectric loss derived from the electrical conduction.[25]

Fig. 2c displays the leakage current density of PMP films. It is clearly seen that introducing an MgO interlayer can remarkably reduce the leakage current compared to pristine PEI films. At 150 °C and 100 MV m^{-1}, the leakage current densities are 1.16×10^{-6} A cm^{-2}, 9.02×10^{-7} A cm^{-2}, 7.71×10^{-7} A cm^{-2}, 4.19×10^{-7} A cm^{-2}, 5.73×10^{-7} A cm^{-2}, respectively, for pristine PEI, PMP-1, PMP-3, PMP-5 and PMP-7 films. The suppressed leakage current density may be good for promoting the electric field endurance and also reducing the energy loss of PMP films at elevated temperature. Furthermore, the empirical model of Schottky emission, $\ln\frac{J}{T^2} = \frac{\sqrt{e^3/4\pi\varepsilon}}{k_B T}\sqrt{E} + \ln A - \frac{\varnothing}{k_B T}$, is used to study the conduction mechanism.[10] The larger intercept of the fitted curve corresponds to the higher barrier height Ø, it can be seen by inserting an inorganic MgO interlayer that the barrier height is significantly improved. In this study, the bandgap structure of PEI and MgO were characterized and are displayed in Fig. S7 (ESI†), it can be seen that the interfacial potential barrier is formed due to the different Fermi level in PEI and MgO, which is beneficial for blocking the charge carrier transport. Different from growing an inorganic layer between the electrode/dielectric interface,[10,21,22] the MgO interlayer is far from the electrode/dielectric interfaces. As we know, it was reported that PEI/$Ca_2Nb_3O_{10}$/PEI sandwiched fillers could form a local electric field due to the different charged state of PEI and $Ca_2Nb_3O_{10}$, this local electric field is inverse to the applied external electric field, which can slow down and block the electrons.[27] In addition, the continuous inorganic interlayer with superior insulation can provide a compact topological barrier to impede the charge transport and reduce the leakage current.[25]

The electric breakdown strength is an important parameter to assess the insulation of dielectric films, which is commonly studied using a two-parameter Weibull distribution function: $P(E) = 1 - \exp\left(\frac{E}{E_b}\right)^{\beta}$, where $P(E)$ is the probability of electric breakdown, E is the measured electric breakdown strength, and E_b is the Weibull breakdown strength defined as $P(E)$ = 63.2%, and β is the shape parameter to evaluate the scatter of the experimental data.[28] The Weibull distribution and E_b values of PMP films are displayed in Fig. 2e. It can be seen that with increasing thickness of the MgO interlayer, at 150 °C, E_b increases at first and then decreases – from 506.7 MV m^{-1}, 513.9 MV m^{-1}, 532.4 MV m^{-1}, 573.1 MV m^{-1} to 537.9 MV m^{-1} for PMP-1–PMP-7 films, respectively. The optimal value of E_b is obtained in the PMP-5 film, which is 1.31 times that of the pristine PEI film. Besides, the β values of PMP films are higher than 10, meaning a good reliability of the resultant films. In order to further confirm the positive effectiveness of the inorganic functional interlayer for improving the electric breakdown strength, PEI films with a BN interlayer (denoted as PBP) were prepared. The optimal E_b value is achieved in the PBP-5 film, which is slightly lower than PMP-5 film due to the lower bandgap and dielectric constant of BN compared with MgO – BN are not aligned in the film direction.[25,29–31] In contrast, PEI filled with BN (denoted as PEI/BN) films is inferior to the E_b of PBP films as given in Fig. S8, ESI,† suggesting that the inorganic fillers agglomeration and electric field concentration between fillers/matrix interfaces may lead to the degradation of breakdown strength. Notably, the E_b of PMP-5 is even greater than that of the other high temperature dielectric films coated with wide bandgap inorganic layers, as shown in Fig. 2f.

To further reveal the mechanism for the reduced leakage current and enhanced breakdown strength of the PMP films, we employ a finite-element method to qualitatively study the electric field distribution and charge carrier behaviors in the PMP films. As shown in Fig. 3a and b, it can be seen that the low electric field region is formed in the MgO layer due to the different electrical properties of PEI and MgO, which means that more energy is needed for electric to pass through the MgO layer. Furthermore, the distribution of charge density is

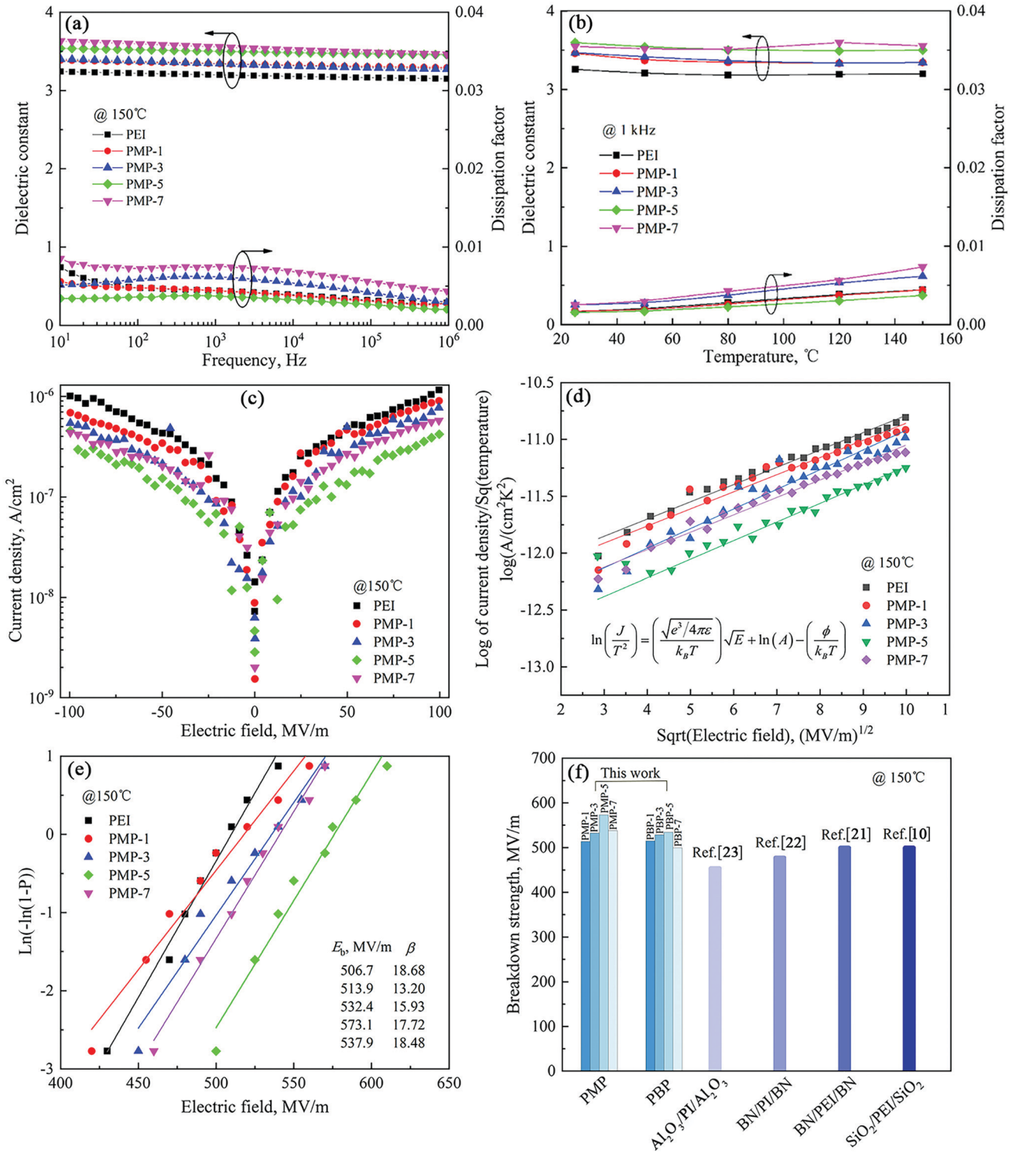

Fig. 2 (a) Frequency-dependent, measured at 150 °C, and (b) temperature-dependent, measured at 1 kHz, dielectric properties of the PMP films. Leakage current density of (c) PMP films measured at an applied field of 100 MV m^{-1} and 150 °C and (d) Schottky plot of PMP films corresponding to (c). (e) Weibull breakdown strength of PMP films measured at 150 °C. (f) Comparison of electric breakdown strength of PMP films with other representative modified-polymer films at 150 °C.

simulated and is displayed in Fig. 3c and d. Since MgO is more insulating and of lower electron mobility than PEI, the MgO layer could be seen as a barrier to hinder the further migration of charge. With the increase of time, the charge transfer in pure PEI film forms a conductive current under the applied electric field. The charge transfer is impeded and concentrated at the

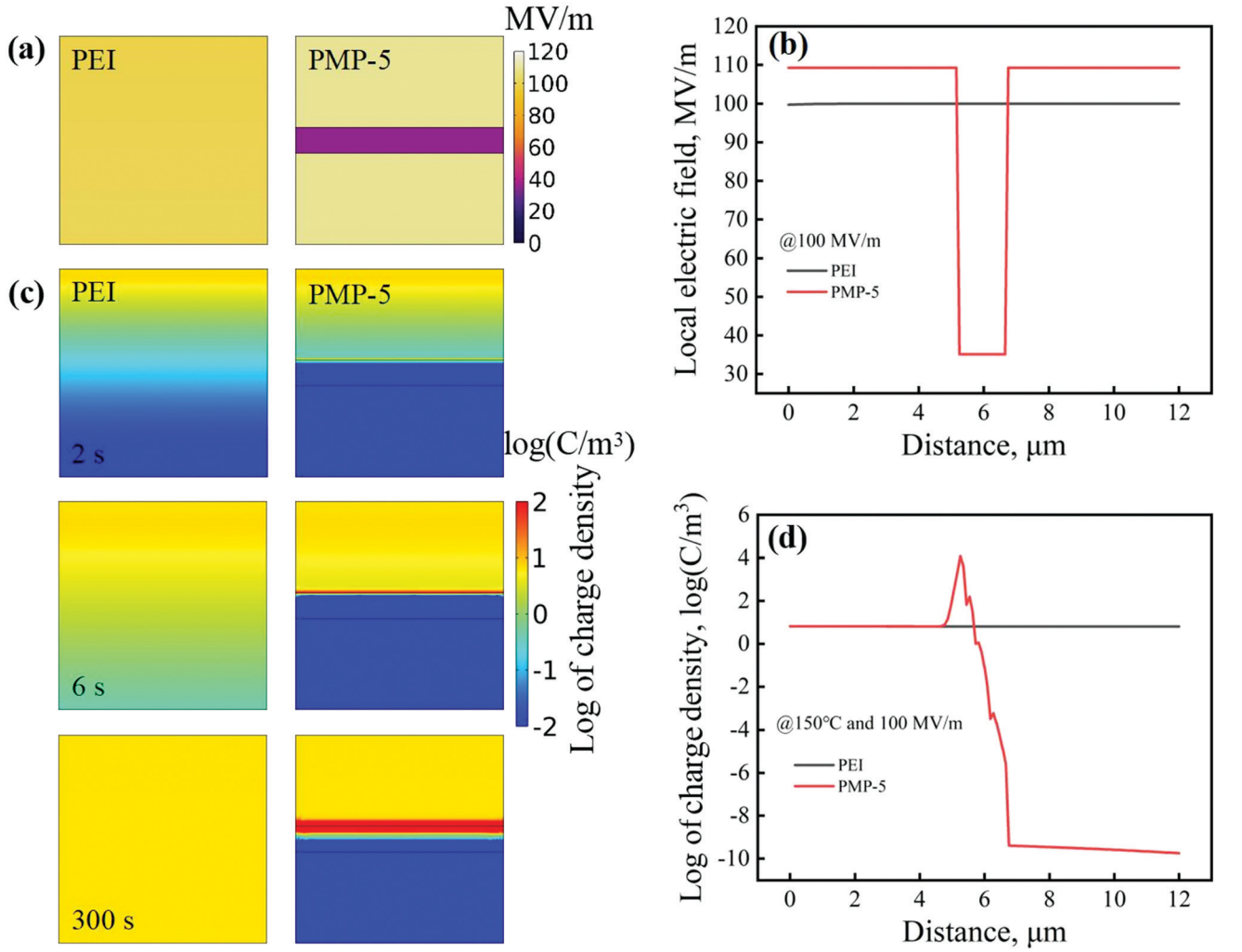

Fig. 3 (a) Simulated electric field distribution of PEI and PMP-5. (b) Local electric field of PEI and PMP-5 along the vertical direction. (c) Simulated charge density distribution of PEI and PMP-5 with increasing time. (d) Local charge density of PEI and PMP-5 along the vertical direction at 300 s.

interface due to the existence of the MgO layer in PMP films, which could effectively reduce the conduction loss. Therefore, both the suppressed leakage current and redistribution of electric field eventually lead to the enhancement of the E_b and η of PMP films.

3.3. Energy storage performance of PMP films

The unipolar hysteresis loops of PMP films at 150 °C were measured using a modified Sawyer-Tower circuit with a 10 Hz triangle voltage. The discharge energy density U_e and efficiency η can be obtained by calculating the integral area in the loops. The area enclosed by the upper and bottom lines stands for energy loss $(1 - \eta)$. As shown in Fig. 4a, it is evident that with increasing applied electric field, the loops of the pristine PEI film become much broader, indicating the significant electric conduction loss and accompanying steep increase in remnant polarization (P_r). In contrast, the loops of the PMP-5 film are much slimmer, as shown in Fig. 4b, suggesting that the MgO interlayer is efficient in reducing the energy loss of the PEI film under high electric fields and high temperature. In detail, it can be seen from Fig. 4c that the P_r value of the pristine PEI film increases from 1.6×10^{-4} C m^{-2} to 0.0074 C m^{-2} with increasing applied electric field, indicating that conduction loss becomes dominant. However, the P_r value of the PMP-5 film merely increases to 0.0012 C m^{-2} at 500 MV m^{-1}, which is beneficial to achieving a high η. Importantly, the deviation value, P_m–P_r, of the maximum polarization (P_m) and P_r determines U_e of the films, in which the PMP-5 film is significantly superior to that of the pristine PEI film, meaning that a high performing U_e at 150 °C would be obtained in PMP films.

In order to better understand the effect of temperature on the energy storage performances of the resultant films, Fig. 4d and e summarize the U_e and η for pristine PEI and PMP-5 films at selected temperatures. When temperature increases from 80 °C to 150 °C, both the U_e and η of the PEI film drop precipitously owing to the increase in electrical conduction and the decrease in electric field endurance, where a U_e is 4.52 J cm^{-3} with an η of 86.47% at 80 °C, and a U_e of 2.46 J cm^{-3} with an η of 44.41% at 150 °C. As expected, although the endurable electric field for PMP-5 film reduces and then leads

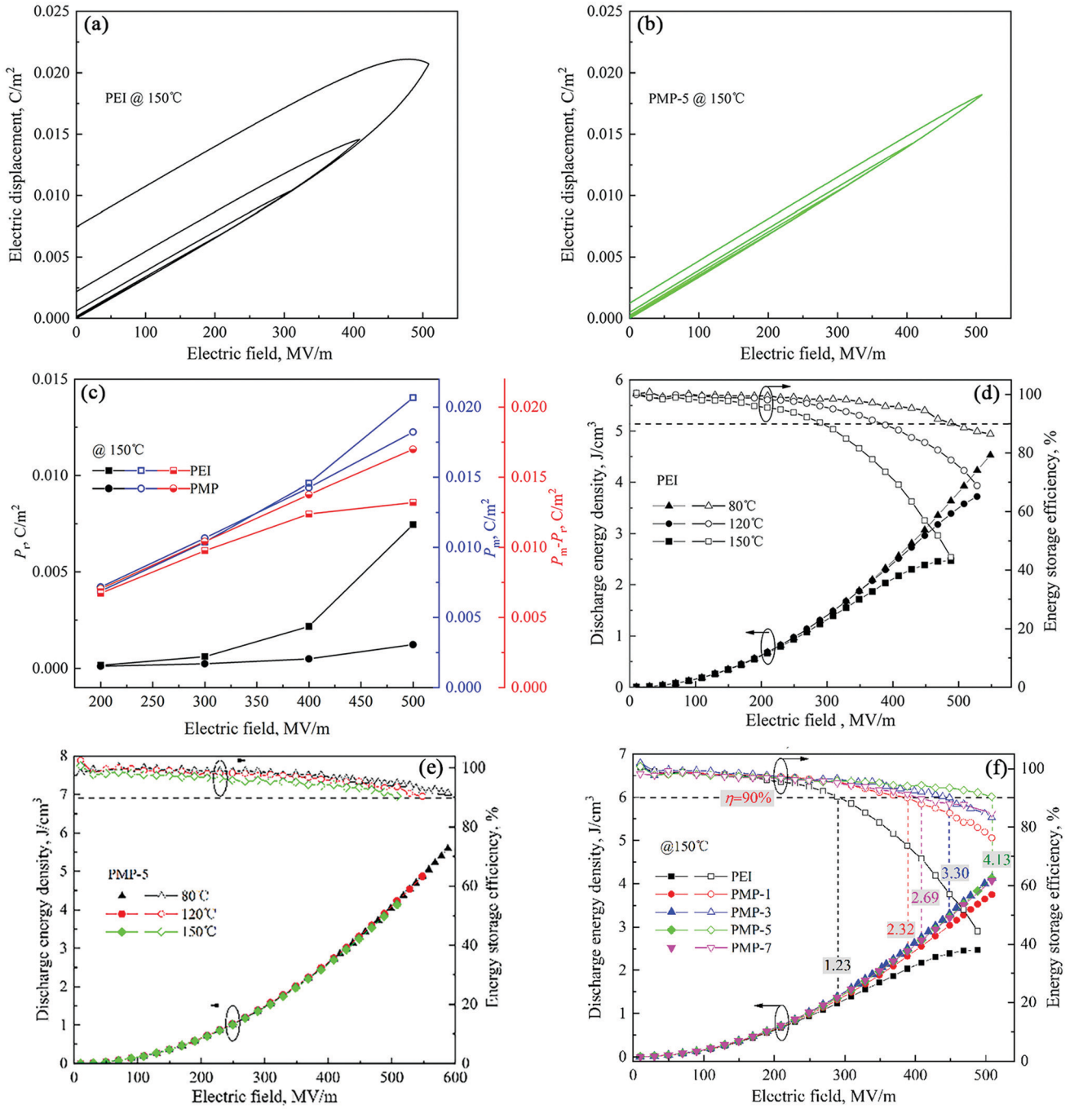

Fig. 4 Hysteresis loops measured at 150 °C of (a) pristine PEI film and (b) PMP-5 film. (c) Comparison of polarization parameters derived from hysteresis loops measured at 150 °C of PEI and PMP-5 films under various electric fields. Discharged energy density and efficiency of (d) pristine PEI film and (e) PMP-5 film at various temperatures. (f) Discharged energy density and efficiency of various PMP films measured at 150 °C.

to a decrease in U_e from 5.59 J cm^{-3} at 80 °C to 4.13 J cm^{-3} at 150 °C, increasing the temperature from 80 °C to 150 °C, the η of PMP-5 film is still above 90% at selected temperatures, indicating that the MgO interlayer can greatly improve capacitive performances, especially discharge efficiency, in comparison to the untreated pristine PEI film at elevated temperatures. As the energy loss would induce undesirable thermal runaway, it is more valuable to evaluate U_e at a high η, *e.g.*, above 90%. As displayed in Fig. 4f, the PMP films all show great improvement in both U_e and η at 150 °C compared with pristine PEI films. In particular, the U_e of PMP-5 at $\eta > 90\%$ is 4.13 J cm^{-3}, almost 3.5 times that of the pristine PEI film (1.23 J cm^{-3}) and about 54 times that of the BOPP film (0.076 J cm^{-3} at 120 °C).[10] To demonstrate the broad effectiveness of this method, the BN inorganic functional layer was also introduced into PEI as an interlayer, where the PBP films exhibit much superior

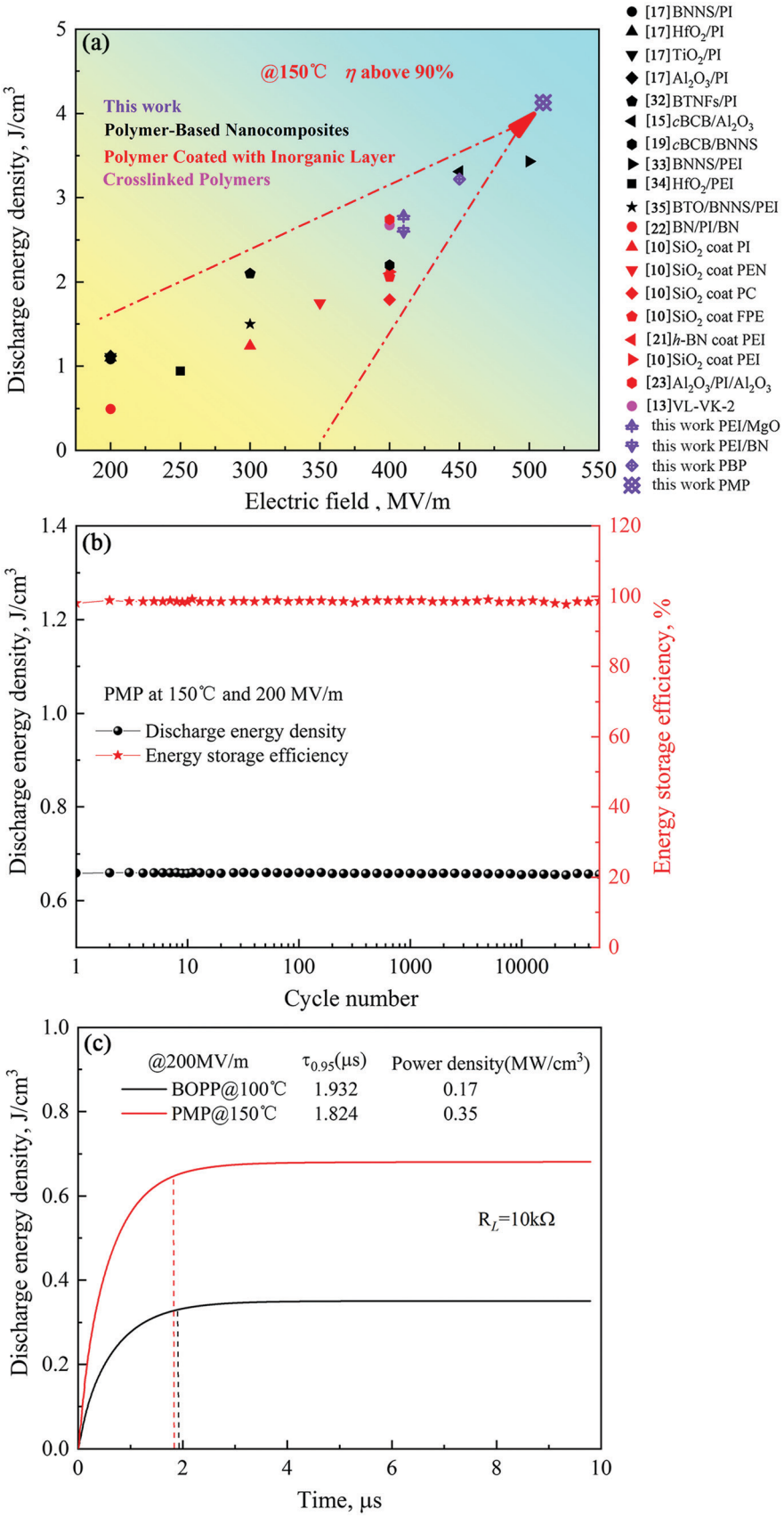

Fig. 5 (a) Comparison of maximum discharge energy density of PMP films in this and previously reported work. (b) Cyclic performance of PMP-5 film at 150 °C and 200 MV m^{-1}. (c) Discharge energy density as a function of time measured from the direct charge of pristine BOPP and PMP-5 films to a 10 kΩ resistor load.

capacitive performance at 150 °C, the U_e of the PBP-5 film at $\eta > 90\%$ is 3.21 J cm^{-3}. It should also be noted that both the U_e at 150 °C of PMP and PBP films are superior to that of PEI/MgO (2.77 J cm^{-3}) and PEI/BN (2.6 J cm^{-3}) nanocomposites with an η above 90%, as shown in Fig. S9, ESI.†

3.4. Comparison with other polymer films and cyclic/fast discharge performances of PMP films

As mentioned in the introduction, some representative strategies have been put forward to improve the capacitive performance of dielectric films at elevated temperature, so we make a comparison and show the results in Fig. 5a.

At 150 °C, the U_e of the PMP-5 film with an η above 90% exceeds the polymer nanocomposites (black color),[15,17,19,32–35] the polymer films coated with a barrier layer (red color),[10,21–23] and the crosslinked polymer (pink color).[13] To the best of our knowledge, a U_e of 4.13 J cm^{-3} with an $\eta > 90\%$ is the maximum value reported so far in polymer-based dielectric films at 150 °C. Besides, due to the capacitors always repeatedly undergoing a charge/discharge process, the cyclic test is essential to evaluate the long-term reliability of the dielectric films. Fig. 5b shows continuous 50 000 cycles of charge/discharge at 150 °C and 200 MV m^{-1}, the U_e and η for the PMP-5 film are almost unchanged, meaning that the PMP-5 film possesses outstanding cyclic stability of capacitive performance and good adhesion between MgO and PEI layers, as shown in Fig. S10, ESI.† Moreover, one of the distinguishing performances of dielectric capacitors compared with batteries is their fast discharge capability. Here, a fast discharge experiment was performed to study the charge/discharge power density of the dielectric films. First, the dielectric films need to be charged with an electric field of 200 MV m^{-1}, then the stored electrical energy discharges to a 10 kΩ resistor load. The discharge time is defined as the time for the discharge energy in a resistor load to reach 95% of the total discharge energy.[36] It can be seen that the discharge time is 1.824 μs for the PMP-5 film at 150 °C and 200 MV m^{-1}, comparable to the commercial BOPP film with a discharge time of 1.932 μs. In particular, the power density for the PMP-5 film is 0.35 MW cm^{-3}, which is twice as much as the BOPP film (0.17 MW cm^{-3}), suggesting the great potential of PMP films to be used in power electronics and electrical systems as high temperature capacitors.

Conclusion

In summary, we have successfully fabricated dielectric films with high temperature capacitive performance. An inorganic functional layer, MgO, with wide bandgap was introduced and served as an interlayer, which enables the PEI films to have reduced leakage current density and improved breakdown strength at high temperatures. The obtained PMP films exhibit excellent capacitive performance; the U_e of the PMP-5 film at $\eta > 90\%$ is 4.13 J cm^{-3} and is almost 3.5 times that of the pristine PEI film (1.23 J cm^{-3}). Besides, the cyclic test confirms that the PMP dielectric films possess good long-term reliability over 50 000 charge/discharge cycles, and also deliver outstanding power density at elevated temperature. All these results encourage us to envision that this simple and effective method would be widely used to develop dielectric films with superior capacitive performance at elevated temperature and high electric field.

Conflicts of interest

There are no conflicts to declare.

Acknowledgements

This work was supported by the National Natural Science Foundation of China (No. 51807042), the Outstanding Youth Fund of Heilongjiang Province (No. YQ2020E031), the China Postdoctoral Science Foundation (No. 2021T140166 and 2018M640303), and the Youth Innovative Talents Training Plan of Ordinary Undergraduate Colleges in Heilongjiang (No. UNPYSCT-2020178).

References

1 M. F. Guo, J. Y. Jiang, Z. H. Shen, Y. H. Lin, C. W. Nan and Y. Shen, *Mater. Today*, 2019, **29**, 49.
2 D. Q. Tan, *Adv. Funct. Mater.*, 2020, **30**, 1808567.
3 X. Y. Huang, B. Sun, Y. K. Zhu, S. T. Li and P. K. Jiang, *Prog. Mater. Sci.*, 2019, **100**, 187.
4 H. Li, F. H. Liu, B. Y. Fan, D. Ai, Z. R. Peng and Q. Wang, *Small Methods*, 2018, **2**, 1700399.
5 J. Chen, Z. H. Shen, Q. Kang, X. S. Qian, S. T. Li, P. K. Jiang and X. Y. Huang, *Sci. Bull.*, 2021, DOI: 10.1016/j.scib.2021.10.011.
6 S. Q. Wang, J. Chen, Y. K. Zhu, P. K. Jiang and X. Y. Huang, *Acta Polym. Sin.*, 2021, **52**, 1148.
7 H. Li, Y. Zhou, Y. Liu, L. Li, Y. Liu and Q. Wang, *Chem. Soc. Rev.*, 2021, **50**, 6369.
8 Q. Li, F. Z. Yao, Y. Liu, G. Z. Zhang, H. Wang and Q. Wang, *Annu. Rev. Mater. Res.*, 2018, **48**, 219.
9 B. Y. Fan, F. H. Liu, G. Yang, H. Li, G. Z. Zhang, S. L. Jiang and Q. Wang, *IET Nanodielectr.*, 2018, **1**, 32.
10 Y. Zhou, Q. Li, B. Dang, Y. Yang, T. Shao, H. Li, J. Hu, R. Zeng, J. L. He and Q. Wang, *Adv. Mater.*, 2018, **30**, 1805672.
11 Z. B. Zhang, D. H. Wang, M. H. Litt, L. S. Tan and L. Zhu, *Angew. Chem.*, 2018, **130**, 1544.
12 Z. B. Zhang, J. F. Zheng, K. Premasiri, M. H. Kwok, Q. Li, R. P. Li, S. B. Zhang, M. H. Litt, X. P. A. Gao and L. Zhu, *Mater. Horiz.*, 2020, **7**, 592.
13 H. Li, M. R. Gadinski, Y. Q. Huang, L. L. Ren, Y. Zhou, D. Ai, Z. B. Han, B. Yao and Q. Wang, *Energy Environ. Sci.*, 2020, **13**, 1279.
14 C. Wu, A. A. Deshmukh, Z. Z. Li, L. H. Chen, A. Alamri, Y. F. Wang, R. Ramprasad, G. A. Sotzing and Y. Cao, *Adv. Mater.*, 2020, **32**, 2000499.

15 H. Li, D. Ai, L. L. Ren, B. Yao, Z. B. Han, Z. H. Shen, J. J. Wang, L. Q. Chen and Q. Wang, *Adv. Mater.*, 2019, **31**, 1900875.
16 T. Zhang, X. Chen, Y. Thakur, B. A. Lu, Q. Y. Zhang, J. Runt and Q. M. Zhang, *Sci. Adv.*, 2020, **6**, eaax6622.
17 D. Ai, H. Li, Y. Zhou, L. L. Ren, Z. B. Han, B. Yao, W. Zhou, L. Zhao, J. M. Xu and Q. Wang, *Adv. Energy Mater.*, 2020, **10**, 1903881.
18 Y. Zhou, C. Yuan, S. J. Wang, Y. J. Zhu, S. Cheng, X. Yang, Y. Yang, J. Hu, J. L. He and Q. Li, *Energy Storage Mater.*, 2020, **28**, 255.
19 Q. Li, L. Chen, M. R. Gadinski, S. H. Zhang, G. Z. Zhang, H. Y. U. Li, E. Iagodkine, A. Haque, L. Q. Chen, T. N. Jackson and Q. Wang, *Nature*, 2015, **523**, 576.
20 C. Yuan, Y. Zhou, Y. J. Zhu, J. J. Liang, S. J. Wang, S. M. Peng, Y. S. Li, S. Cheng, M. C. Yang, J. Hu, B. Zhang, R. Zeng, J. L. He and Q. Li, *Nat. Commun.*, 2020, **11**, 1.
21 A. Azizi, M. R. Gadinski, Q. Li, M. A. AlSaud, J. J. Wang, Y. Wang, B. Wang, F. H. Liu, L. Q. Chen, N. Alem and Q. Wang, *Adv. Mater.*, 2017, **29**, 1701864.
22 S. Cheng, Y. Zhou, J. Hu, J. L. He and Q. Li, *IEEE Trans. Dielectr. Electr. Insul.*, 2020, **27**, 498.
23 J. F. Dong, R. C. Hu, X. W. Xu, J. Chen, Y. J. Niu, F. Wang, J. Y. Hao, K. Wu, Q. Wang and H. Wang, *Adv. Funct. Mater.*, 2021, **31**, 2102644.
24 Q. Li, F. H. Liu, T. N. Yang, M. R. Gadinski, G. Z. Zhang, L. Q. Chen and Q. Wang, *Proc. Natl. Acad. Sci. U. S. A.*, 2016, **113**, 9995.
25 Y. K. Zhu, Y. J. Zhu, X. Y. Huang, J. Chen, Q. Li, J. L. He and P. K. Jiang, *Adv. Energy Mater.*, 2019, **9**, 1901826.
26 F. Dumludag, D. Bakay and A. Altindal, *AIP Conf. Proc.*, 2010, **1203**, 533.
27 Z. W. Bao, C. M. Hou, Z. H. Shen, H. Y. Sun, G. Q. Zhang, Z. Luo, Z. Z. Dai, C. M. Wang, X. W. Chen, L. B. Li, Y. W. Yin, Y. Shen and X. G. Li, *Adv. Energy Mater.*, 2020, **32**, 1907227.
28 H. F. Li, L. W. Wang, Y. K. Zhu, P. K. Jiang and X. Y. Huang, *Chin. Chem. Lett.*, 2021, **32**, 2229.
29 S. Heo, E. Cho, H. I. Lee, G. S. Park, H. J. Kang, T. Nagatomi, P. Choi and B. D. Choi, *AIP Adv.*, 2015, **5**, 077167.
30 Y. Chen, Q. Kang, P. K. Jiang and X. Y. Huang, Rapid, *Nano Res.*, 2021, **14**, 2424.
31 S. Cheng, Y. Zhou, Y. S. Li, C. Yuan, M. C. Yang, J. Fu, J. Hu, J. L. He and Q. Li, *Energy Storage Mater.*, 2021, **42**, 445.
32 P. H. Hu, W. D. Sun, M. Z. Fan, J. F. Qian, J. Y. Jiang, Z. K. Dan, Y. H. Lin, C. W. Nan, M. Li and Y. Shen, *Appl. Surf. Sci.*, 2018, **458**, 743.
33 H. X. Chen, Z. B. Pan, W. L. Wang, Y. Y. Chen, S. Xing, Y. Cheng, X. P. Ding, J. J. Liu, J. W. Zhai and J. H. Yu, *Composites, Part A*, 2021, **142**, 106266.
34 L. L. Ren, L. J. Yang, S. Y. Zhang, H. Li, Y. Zhou, D. Ai, Z. l. Xie, X. T. Zhao, Z. R. Peng, R. J. Liao and Q. Wang, *Compos. Sci. Technol.*, 2021, **201**, 108528.
35 H. Li, L. L. Ren, D. Ai, Z. B. Han, Y. Liu, B. Yao and Q. Wang, *InfoMat*, 2020, **2**, 389.
36 P. Khanchaitit, K. Han, M. R. Gadinski, Q. Li and Q. Wang, *Nat. Commun.*, 2013, **4**, 2845.

